

Distributed Semantic Segmentation with Efficient Joint Source and Task Decoding

Danish Nazir^{1,2}, Timo Bartels¹, Jan Piewek², Thorsten Bagdonat², and Tim Fingscheidt¹

¹ Technische Universität Braunschweig, Braunschweig, Germany
{danish.nazir,timo.bartels,t.fingscheidt}@tu-bs.de

² Group Innovation, Volkswagen AG, Wolfsburg, Germany
{danish.nazir,jan.piewek,thorsten.bagdonat}@volkswagen.de

Abstract. Distributed computing in the context of deep neural networks (DNNs) implies the execution of one part of the network on edge devices and the other part typically on a large-scale cloud platform. Conventional methods propose to employ a serial concatenation of a learned image and source encoder, the latter projecting the image encoder output (bottleneck features) into a quantized representation for bitrate-efficient transmission. In the cloud, a respective source decoder reprojects the quantized representation to the original feature representation, serving as an input for the downstream task decoder performing, e.g., semantic segmentation. In this work, we propose *joint* source and task decoding, as it allows for a *smaller network size in the cloud*. This further enables the scalability of such services in large numbers without requiring extensive computational load on the cloud per channel. We demonstrate the effectiveness of our method by achieving a distributed semantic segmentation SOTA over a wide range of bitrates on the mean intersection over union metric, while using only 9.8% ... 11.59% of cloud DNN parameters used in previous SOTA on the COCO and Cityscapes datasets.

Keywords: Feature Compression · Distributed Semantic Segmentation

1 Introduction

Deep neural networks (DNNs) have been very successful in performing machine perception tasks, including semantic segmentation [12, 22, 32, 37]. Due to a surge in camera-enabled edge devices with limited computational capabilities across various application fields, such as smart transportation, agriculture, and manufacturing, improving the task efficiency of powerful segmentation DNNs is very important [2, 6, 41]. However, since there is a trend towards an increasing size and complexity of advanced DNN architectures, it is difficult to execute them on edge devices due to both power and computational complexity limitations [17]. Accordingly, current approaches [1, 6, 33, 34] propose to distribute the execution of segmentation DNNs into two parts, where one part of the DNN is executed on the edge device and the other on a large-scale cloud platform.

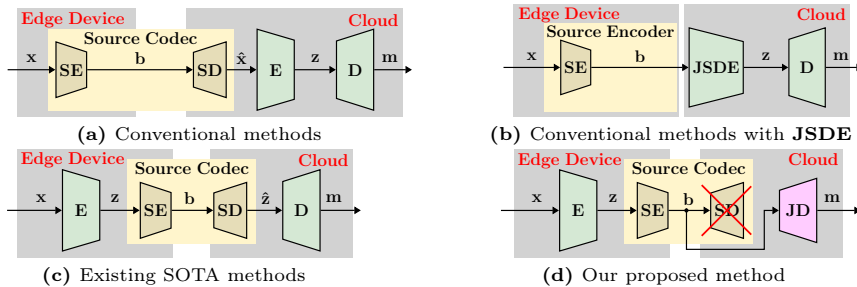


Fig. 1: High-level comparison of our proposed approach with existing SOTA approaches in distributed semantic segmentation. Here, **SE** and **SD** represent the source encoder and decoder, respectively. Blocks **E** and **D** are the image encoder and task decoder, respectively. Further, **JSDE** is the joint source decoder and image encoder, while **JD** represents the proposed joint source and task decoder, in short: joint decoder.

As shown in Figure 1a, the conventional solution is to deploy a source encoder **SE** on the edge device and a source decoder **SD** along with image encoder **E** and task decoder **D** in the cloud. Both, traditional codecs, such as JPEG [46] and HEVC [40], and learned image codecs [4, 35, 39] can be employed as source codec. The **SE** outputs a quantized compressed bitstream b , which is transmitted to the cloud. Although the conventional solution involves deployment of low-complex **SE** on an edge device, executing the three functions **SD**, **E**, and **D** in the cloud prohibits scalability of such service. Furthermore, image compression requires a higher bitrate [1, 34] and it also compromises potential data protection requirements as images can be reproduced anywhere from the bitstream.

As shown in Figure 1b, one can merge **SD** and **E**, while the edge device computational complexity stays the same as in Figure 1a [30, 43, 48]. However, this approach may reduce the computational complexity in the cloud by utilizing a joint source decoder and image encoder **JSDE**. Similar to the conventional solution described in Figure 1a, it also faces the data protection problem and still requires a relatively high bitrate.

As shown in Figure 1c, the current state-of-the-art (SOTA) approach [1] deploys **E** and a low-complex **SE** on the edge device. Ahuja et al. [1] aim at compressing the bottleneck features z based on the same principles as learned image codecs [38]. Compared to conventional approaches as described in Figures 1a and 1b, this incurs a slightly higher computational complexity on the edge device but with the advantage that this method is more bitrate efficient. Additionally, it requires a lower computational complexity in the cloud and the data protection problem is also largely solved, as, in the case of a semantic segmentation task, only the segmentation masks can be retrieved on the receiver side, but the original image x cannot be reconstructed with sufficient fidelity.

As shown in Figure 1d, inspired by the idea of joint functions in Figure 1b, we propose to perform *joint source and task decoding* using **JD**, joint decoding. It

allows even lower computational complexity in the cloud, while achieving superior rate-distortion (RD) performance. Further, it enables to scale such service to millions of edge devices, keeping the edge device’s computational complexity of our proposed approach the same as the so-far SOTA (Figure 1c).

Our contribution with this work on distributed semantic segmentation is threefold. First, we propose to perform joint source and task decoding, which results in a computationally highly efficient cloud DNN, enabling us to perform distributed semantic segmentation at a very large scale without requiring extensive computational load per channel. Secondly, instead of applying training-time over-parameterization in the image encoder as suggested by [16, 44, 45], we employ it in our proposed joint decoder **JD**, which takes quantized bottleneck features as input, to further enhance the performance in the high-bitrate regime. Finally, we set a new distributed semantic segmentation SOTA benchmark over a wide range of bitrates on the mean intersection over union (mIoU) metric, while using only 9.8% of the cloud DNN parameters on COCO, and 11.59% on the Cityscapes dataset, compared to previous SOTA [1].

2 Related Works

In this section, we start by discussing general DNN-based semantic segmentation methods, followed by previous research in the distributed setting.

2.1 Semantic Segmentation

As a fundamental computer vision task, semantic segmentation aims to classify each pixel of an image with a set of categories. Since the advent of DNNs [23, 26], fully convolutional networks (FCNs) [32, 37] have achieved SOTA on various segmentation benchmarks [11, 18, 29, 54]. After that, researchers shifted their focus on refining FCNs through various aspects, including exploitation of contextual information [12, 22], introduction of image pyramids [7, 9] and pooling [20, 28], development of enhanced receptive fields [13, 50]. Nowadays, transformer-based [21, 24, 51] and multi-modal foundation models [47, 48] dominate the semantic segmentation benchmarks.

2.2 Distributed Semantic Segmentation

General: Over the past few years, several approaches proposed to distribute the execution of the semantic segmentation DNN over a client/server architecture [30, 43, 49]. All of them share a common idea, which is to utilize a pre-trained learned image compression method as source codec [4] and use the source encoder output, i.e., the quantized compressed latent space, to perform joint source decoding and image encoding through **JSDE**. As shown in Figure 1b, the output of **JSDE** is sent to a task decoder **D** to produce a semantic segmentation map. Both **JSDE** and **D** together form a semantic segmentation DNN, operating on a compressed bitstream **b**. Typically, in the first step, the source codec is

trained, and in the second step, the semantic segmentation DNN is trained on the output of the pre-trained source encoder. The choice for a semantic segmentation DNN in conventional approaches [30,43,49] is DeepLabv3 [8], but a problem arises, as the size of the quantized compressed latent space is not suitable for its ResNet-50 encoder. As a solution, they either use transposed convolutional layers [30,43] or pixel shuffling [49] for upsampling it to meet the ResNet-50 input dimensions, while removing the initial two layers. Furthermore, some approaches [30,31] employ feature selection mechanisms and supervision based on knowledge distillation (KD) to further enhance the RD performance. Their semantic segmentation DNN is fully executed in the cloud, while the source encoder is deployed on the edge device with limited computational demands.

Low-complexity encoder-decoder setup: In contrast to the conventional distributed semantic segmentation approaches outlined above, current SOTA methods [1,14,19,34] propose to apply the source codec *within* the DeepLabv3 ResNet-50 encoder or between the ResNet-50 and DeepLabv3 task decoder as shown in Figure 1c, to compress features instead of focusing on image compression. This results in two benefits: (1) There is no need for a pre-trained learned image codec, as compression will be applied directly on feature level and trained in an end-to-end manner. (2) The source decoder (**SD**) becomes smaller, thus enhancing the scalability of the service. We build upon the setup of current SOTA approaches and focus on making the cloud DNNs even more efficient by performing *joint source and task decoding* with a single joint decoder DNN **JD**, cf. Figure 1d. This further increases the scalability of performing semantic segmentation in a distributed computing paradigm. Furthermore, we improve performance in the high-bitrate regime by introducing re-parameterizable branches in the joint decoder **JD** via the re-parameterization trick on the quantized features [16,44].

3 Method

In this section, we first describe the feature compression method. Afterwards, we discuss our proposed approach for joint source and task decoding followed by training-time over-parameterization.

3.1 Bottleneck Feature Compression with Variational Models

Image compression works [3,4,53] have shown that the rate-distortion (RD) objective of lossy compression can be formulated as a variational autoencoder (VAE) [25]. Similarly, recent works [1,19,34] have adapted the same framework and proposed to use a source codec for compressing the bottleneck features $\mathbf{z} = \mathbf{E}(\mathbf{x}; \boldsymbol{\theta}^E)$ from image encoder \mathbf{E} with parameters $\boldsymbol{\theta}^E$. Here, $\mathbf{x} = (\mathbf{x}_i) \in \mathbb{I}^{H \times W \times C}$ is a normalized image of height H , width W , and $C = 3$ color channels, with pixel $\mathbf{x}_i \in \mathbb{I}^C$, pixel index $i \in \mathcal{I}$, pixel index set $\mathcal{I} = \{1, \dots, H \cdot W\}$

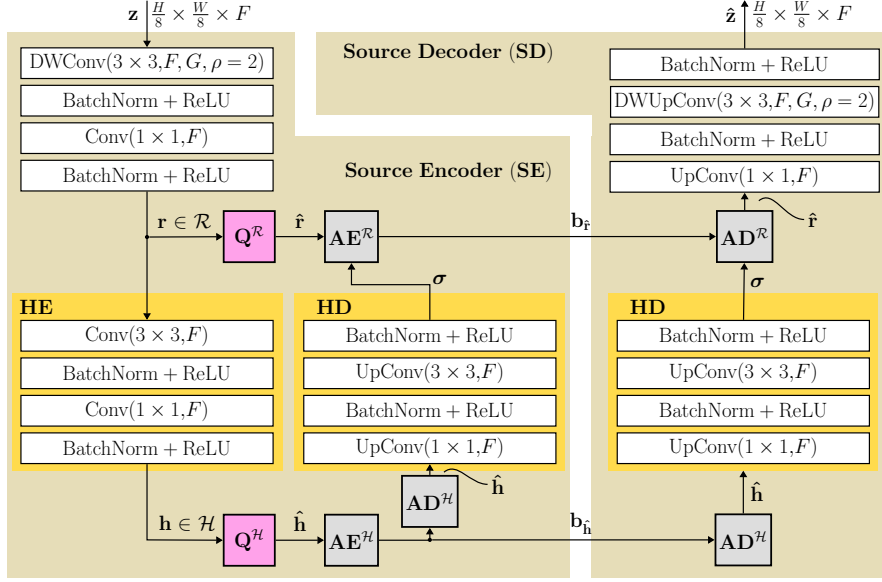


Fig. 2: Hyperprior architecture of source encoder **SE** and source decoder **SD**, see [1, 4].

and $\mathbb{I} = [0, 1]$. As shown in Figure 2, the source codec consists of the bottleneck source encoder **SE** with parameters θ^{SE} and the bottleneck source decoder **SD** with parameters θ^{SD} , which follow a hyperprior [4] architecture. The **SE** utilizes a quantizer $\mathbf{Q}^{\mathcal{R}}$ to produce a latent bitstream $\mathbf{b}_{\hat{\mathbf{r}}} = \mathbf{SE}^{(\mathbf{r})}(\mathbf{z}; \theta^{\text{SE}})$, which is entropy-coded using arithmetic coding [27]. However, quantization is a non-differentiable operation, making it impossible to backpropagate during training. Therefore, we need to relax the problem to cast it to a VAE by either replacing the quantization by the smooth approximation of the gradients [42] or by additive uniform noise with a probability density function (PDF) of width one, over the interval $(-\frac{1}{2}, \frac{1}{2})$ [3], given that the elements of $\mathbf{r} \in \mathbb{R}^d$ and the uniform noise are in 32 bit floating point number representation. In our work, we follow the latter method, but switch back to true quantization during inference. The source decoder proceeds by reconstructing the bottleneck features $\hat{\mathbf{z}} = \mathbf{SD}(\mathbf{SE}(\mathbf{z}; \theta^{\text{SE}}); \theta^{\text{SD}})$, which are passed to task decoder **D** resulting in the network prediction $\mathbf{y} = (y_{i,s}) \in \mathbb{I}^{H \times W \times S}$, with classes $\mathcal{S} = \{1, 2, \dots, S\}$, class index $s \in \mathcal{S}$, and number of classes S . The final semantic segmentation map is given as $\mathbf{m} = (m_i)$ with $m_i = \arg \max_{s \in \mathcal{S}} y_{i,s}$. Both, **SE** and **SD**, contain grouped convolutions and grouped transposed convolutions [1], which are denoted by $\text{DWConv}(h \times h, F, G, \rho = 2)$ and $\text{DWUpConv}(h \times h, F, G, \rho = 2)$, respectively, where $h \times h$ is the kernel size, F is the number of kernels, G is the number of groups present in the layer, and stride $\rho = 2$. They also contain regular convolutional and transposed convolutional layers, which are represented by $\text{Conv}(h \times h, F)$ and $\text{UpConv}(h \times h, F)$, respectively.

The elements of bitstream $\mathbf{b}_{\hat{\mathbf{r}}}$ reveal a substantial amount of statistical dependencies and correlations. Accordingly, an enhancement bitstream $\mathbf{b}_{\hat{\mathbf{h}}}$ is being introduced in the source codec to model a time-variant standard deviation vector $\boldsymbol{\sigma}$ for arithmetic coding $\mathbf{AE}^{\mathcal{H}}$ [4]. As shown in Figure 2, it is produced by a hyperprior encoder and a quantizer $\mathbf{Q}^{\mathcal{H}}$ as $\mathbf{b}_{\hat{\mathbf{h}}} = \mathbf{SE}^{(\mathbf{h})}(\mathbf{r}; \boldsymbol{\theta}^{\text{HE}})$. The quantization and entropy coding process to obtain $\mathbf{b}_{\hat{\mathbf{h}}}$ is similar as with $\mathbf{b}_{\hat{\mathbf{r}}}$. Due to the introduction of $\mathbf{b}_{\hat{\mathbf{h}}}$, each element in $\hat{\mathbf{r}}$ can now be modeled as zero-mean Gaussian with its individual standard deviation σ_i using a hyperprior decoder \mathbf{HD} as $\boldsymbol{\sigma} = (\sigma_i) = \mathbf{HD}(\hat{\mathbf{h}}; \boldsymbol{\theta}^{\text{HD}})$ with parameters $\boldsymbol{\theta}^{\text{HD}}$. Note that the entire source encoder can be written as $(\mathbf{b}_{\hat{\mathbf{r}}}, \mathbf{b}_{\hat{\mathbf{h}}}) = \mathbf{SE}(\mathbf{z}; \boldsymbol{\theta}^{\text{SE}})$ and the respective source decoder as $\hat{\mathbf{z}} = \mathbf{SD}(\mathbf{b}_{\hat{\mathbf{r}}}, \mathbf{b}_{\hat{\mathbf{h}}}; \boldsymbol{\theta}^{\text{SD}})$. The expected bitrate during training can be defined as

$$J^{\text{rate}} = \mathbb{E}_{\mathbf{x} \sim p_{\text{train}}} \left[\frac{-\log_2(\mathbb{P}_{\hat{\mathbf{r}}}(\hat{\mathbf{r}}|\hat{\mathbf{h}})) - \log_2(\mathbb{P}_{\hat{\mathbf{h}}}(\hat{\mathbf{h}}))}{H \cdot W} \right], \quad (1)$$

with $\mathbb{E}_{\mathbf{x} \sim p_{\text{train}}}$ representing the expectation over a minibatch in the dataset, $\mathbb{P}_{\hat{\mathbf{r}}}$ and $\mathbb{P}_{\hat{\mathbf{h}}}$ denoting the discrete probability distributions over the quantized latent spaces $\hat{\mathbf{r}}$ and $\hat{\mathbf{h}}$, respectively.

Since the task decoder \mathbf{D} performs semantic segmentation, the distortion objective is formulated as a cross-entropy loss.

$$J^{\text{dist}} = \mathbb{E}_{\mathbf{x} \sim p_{\text{train}}} \left[\frac{1}{|\mathcal{I}|} \sum_{i \in \mathcal{I}} \sum_{s \in \mathcal{S}} \bar{y}_{i,s} \cdot \log(y_{i,s}) \right]. \quad (2)$$

Here, $\bar{\mathbf{y}} = (\bar{y}_{i,s}) \in \{0, 1\}^{H \times W \times S}$ is the one-hot-encoded ground truth and we have $\forall i \in \mathcal{I} : \sum_{s \in \mathcal{S}} y_{i,s} = 1$, $\sum_{s \in \mathcal{S}} \bar{y}_{i,s} = 1$. By combining (1) and (2), we obtain the RD trade-off as follows:

$$J = \alpha \cdot J^{\text{dist}} + (1 - \alpha) \cdot J^{\text{rate}}. \quad (3)$$

The RD trade-off is controlled by the hyperparameter $\alpha \in (0, 1)$. Further, in the case of other downstream tasks such as object detection etc., \mathbf{JD} and J^{dist} in (3) can be replaced by a task-specific decoder and loss, respectively.

3.2 Proposed Joint Source and Task Decoder (JD)

As shown in Figure 1d, and unlike existing approaches [1, 19] in distributed semantic segmentation, we propose to omit the reconstruction of $\hat{\mathbf{z}}$ and redirect the quantized latent space variable $\hat{\mathbf{r}}$ to the proposed joint source and task decoder $\mathbf{JD}(\mathbf{b}_{\hat{\mathbf{r}}}, \mathbf{b}_{\hat{\mathbf{h}}}; \boldsymbol{\theta}^{\text{JD}})$ with parameters $\boldsymbol{\theta}^{\text{JD}}$. Omitting the reconstruction target $\hat{\mathbf{z}}$ does not impede the learning process as shown in (3). The aim of \mathbf{JD} is to perform both source and task decoding at once. Therefore, the bottleneck source decoder \mathbf{SD} is not needed anymore, only the former decoder \mathbf{D} is to be expanded towards a joint source and task decoder to produce the semantic segmentation mask as $\mathbf{m} = \mathbf{JD}(\mathbf{b}_{\hat{\mathbf{r}}}, \mathbf{b}_{\hat{\mathbf{h}}}; \boldsymbol{\theta}^{\text{JD}}) \in \mathbb{I}^{H \times W \times S}$ with classes $\mathcal{S} = \{1, 2, \dots, S\}$, class index $s \in \mathcal{S}$, and number of classes S . The network structure of \mathbf{JD} is shown in

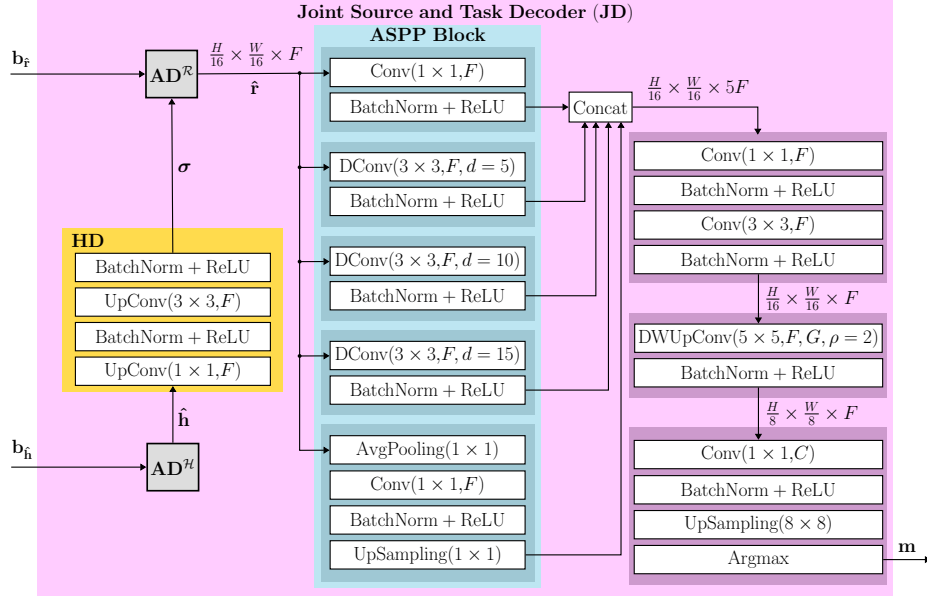


Fig. 3: Proposed architecture of the joint source and task decoder (JD, see Fig. 1d). *Training* details of the blue convolutional blocks within the ASPP block are shown in Figure 4.

Figure 3. The source encoder generates $\mathbf{b}_{\hat{h}}$, which serves as an input to **JD**, alongside the hyperprior bitstream $\mathbf{b}_{\hat{f}}$. Similar to **D**, also **JD** contains an atrous spatial pyramid pooling (ASPP) block [8]. It consists of dilated convolutions, which are denoted by $\text{DConv}(h \times h, F, d)$, where $h \times h$ is the kernel size, F is the number of kernels present in the layer and d is the dilation rate. Separated from the dilated convolutions, it also contains upsampling layers, which are represented by $\text{UpSampling}(u \times v)$, where $u \times v$ is the desired spatial size of the input features. Further, **JD** also contains a single grouped transposed convolution, which is denoted by $\text{DWUpConv}(h \times h, F, G, \rho = 2)$, where $h \times h$ is the kernel size, F is the number of kernels, G is the number of groups present in the layer, and stride $\rho = 2$. However, the key difference between **D** and **JD** remains that **JD** can perform joint source and task decoding. For an easy comparison, we also provide the full diagram of **SD** and **D** of the so-far SOTA (Figure 1c, [1]) in the Supplement Figure 9. Furthermore, our RD optimization problem remains the same as described in (3). Interestingly, we do not enforce **JD** to learn source decoding by utilizing any extra loss terms.

3.3 Training-Time Over-Parameterization

As a consequence of performing joint source and task decoding in **JD**, the number of network parameters is significantly smaller compared to the task decoder

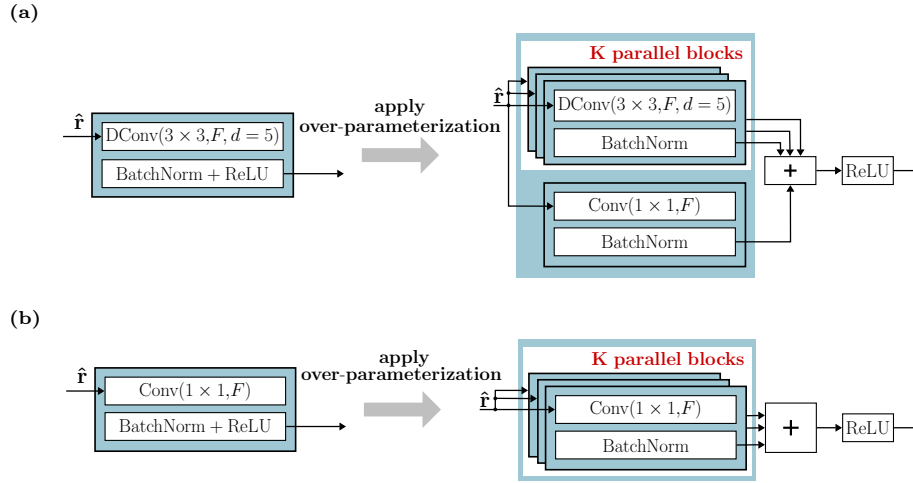


Fig. 4: Proposed over-parameterization of the **JD** ASPP subblocks in Figure 3.

D. For low bitrates, the proposed **JD** outperforms existing SOTA methods, but without further measures we would observe a slight quality decrease at higher bitrates. However, simply increasing the size of **JD** is not desirable, since it must be highly efficient to enable large-scale services in the cloud. Accordingly, to reach superior performance also at high bitrates, we propose to perform training-time over-parameterization [16, 44, 45] by introducing re-parameterizable branches [15, 16] without skip connections in the ASPP block of **JD**. Typically, this is only applied to the encoder **E**. However, since the ASPP block also acts as a feature extractor by extracting features from $\hat{\mathbf{r}}$ at multiple scales through various dilation rates d , it is also possible to perform over-parameterization to the ASPP subblocks. Note that the over-parameterization is applied to **JD** only during training. At inference, the network topology of ASPP block remains as in Figure 3.

Figure 4 presents how to apply training-time over-parameterization to the subblocks of the ASPP block. As depicted in Figure 4a, for all three dilated convolutional subblocks with dilation rates $d \in \{5, 10, 15\}$ of the ASPP block, the dilated convolutional layer along with batchnorm is duplicated into K parallel blocks with indices $k \in \mathcal{K} = \{1, \dots, K\}$. Furthermore, a single pointwise convolutional block [44, 45] is also applied in parallel to the K blocks of the dilated convolutional subblocks, resulting in $K + 1$ parallel branches. The outputs of the in total $K + 1$ parallel branches is summed up and followed by the ReLU activation function. As shown in Figure 4b, for the remaining two convolutional subblocks of the ASPP block (top and bottom), since they contain only pointwise convolutions, the output of K parallel subblocks is summed up [44, 45] and the ReLU activation function is applied on the summed output.

Table 1: Datasets & splits used in our experiments

| Dataset | Official subsets | #Images | Symbol |
|-----------------|------------------|---------|--|
| COCO-2017 [29] | train | 118,287 | $\mathcal{D}_{\text{COCO}}^{\text{train}2017}$ |
| | val | 5,000 | $\mathcal{D}_{\text{COCO}}^{\text{val}2017}$ |
| Cityscapes [11] | train | 2,975 | $\mathcal{D}_{\text{CS}}^{\text{train}}$ |
| | val | 500 | $\mathcal{D}_{\text{CS}}^{\text{val}}$ |

4 Experimental Overview

Following current SOTA methods [1, 19, 34], we also chose DeepLabv3 [8] with a ResNet-50 [23] encoder for conducting all our experiments. DeepLabv3 does not use encoder-decoder skip connections, which enables bitrate-efficient transmission between the edge device and the cloud platform, making it optimal for distributed deployment. Since our proposed **JD** takes the final output of the bottleneck source encoder, we chose the split point right after the ResNet-50 backbone as shown in Supplement Figure 10, which presents the entire edge device processing (transmitter side) in our investigations. For a fair comparison to our approach, we also use the same split point to train the SOTA baseline [1]. All of our experiments and evaluation metrics are implemented using PyTorch [36], the MMSegmentation toolbox [10], and the Compress-AI [5] library. Following previous works [1, 19, 34], we perform our ablation studies and results benchmarking on the validation set. In the following, we introduce the datasets, training and evaluation settings, and the metrics.

4.1 Datasets

We report the results on well-established indoor and outdoor datasets for semantic segmentation, including COCO-2017 [29] and Cityscapes [11]. Typically, in distributed semantic segmentation, COCO-2017 is considered to be most challenging due to its diverse object categories, crowded scenes, scale variation and large size [29, 34]. It also includes pixel-level annotations for **things** and **stuff** categories, enabling the generation of high-quality segmentation masks. Many prior works (e.g., [1, 34, 38]) report results on it. Note that another relevant approach [19] also reported results on Cityscapes. Therefore, in order to be comparable with existing works, we provide results on both datasets. The number of images and split information in respective datasets is shown in Table 1.

4.2 Experimental Design, Training and Metrics

We trained and evaluated all of our models on an NVIDIA V100 GPU. The training resolution for the COCO-2017 dataset is 513×513 [1], whereas for the Cityscapes dataset it is 769×769 [19]. Furthermore, we select 21 classes in COCO-2017 based on the classes in PASCAL-VOC-2012 [18] dataset, as suggested by

important prior works [1, 34, 36, 38]. For the COCO dataset, the number of feature maps F in the ASPP head is 256 [1, 34], while for Cityscapes it is set to 512 [19]. We follow the same training setup as in [1]. However, since **JD** has to perform joint source and task decoding, we update its weights along with **SE** in an end-to-end manner during training. As a starting point in the training, both **JD** and **SE** weights are randomly initialized and we do not use any pre-trained weights. The training setup and all hyperparameters are described in more detail in the Supplement Section 1.

To ensure fair comparison, a recent SOTA learned image codec from Song et al. [39] is fine-tuned to the respective dataset. After fine-tuning, the model weights for Song et al. [39] are fixed. For both datasets, we use the pre-trained NoCompression DeepLabv3 model with a ResNet-50 [23] encoder and fine-tune it based on the compressed images from traditional codecs $\hat{\mathbf{x}} = \mathbf{SD}(\mathbf{b})$ and learned codec $\hat{\mathbf{x}} = \mathbf{SD}(\mathbf{b}; \theta^{\text{SD}})$. The conventional method baselines (Figure 1a) include the traditional codecs JPEG [46], HEVC [40], and a learned codec by Song et al. [39]. Note that for COCO, the results for JPEG and HEVC are from Matsuba et al. [34], whereas for Cityscapes, we obtain the results for JPEG ourselves, while HEVC results are from Feng et al. [19].

For the conventional method with the **JSDE** baseline (Figure 1b), we follow the training recipe from Liu et al. [30] to train the method proposed by Torfason et al. [43]. The **JSDE** follows a ResNet-50 topology, but to utilize the compressed latent variable $\hat{\mathbf{f}}$ as input, the initial convolutions are replaced by transposed convolutions [43], cf. Section 2.2. We use the learned image codec by Ballé et al. [4] from the Compress-AI model zoo, which is pre-trained on the Vimeo-90K [52] dataset. After that, we perform joint fine-tuning of **SE**, **JSDE** and **D** on the respective datasets.

To evaluate the RD performance of all our models, the rate is defined following (1) as bits per pixel (bpp). To measure distortion, we report the mIoU metric, which is prevalent in distributed semantic segmentation methods [1, 31, 34, 43]. Furthermore, we report the number of floating-point operations per image (FLOPs) and the number of parameters.

5 Results and Discussion

In this section, we will first discuss the rate-distortion (RD) performance of our proposed approach and compare it against recent SOTA approaches. Afterwards, we evaluate different model settings through ablation studies to design our final joint decoder (**JD**) for both COCO and Cityscapes datasets.

5.1 Comparison With SOTA Methods

We reproduced the existing SOTA baseline (Figure 1c) from Ahuja et al. [1] on COCO and also obtain it for the Cityscapes dataset. Furthermore, for both datasets, our method’s results and those of Ahuja et al. [1] are averaged over three different random seeds. However, for different random seeds, resulting RD

Table 2: Comparison of FLOPs and #params (cloud DNNs)

| Methods | COCO | | Cityscapes | |
|---------------------------|-----------|-------------|------------|-------------|
| | FLOPs (G) | #params (M) | FLOPs (G) | #params (M) |
| Song et al. [39] (1a) | 1386 | 67.21 | 2834 | 93.30 |
| Torfason et al. [43] (1b) | 734 | 43.23 | 1153 | 69.32 |
| Ahuja et al. [1] (1c) | 521 | 16.78 | 1366 | 42.44 |
| Ours (1d) | 10 | 1.66 | 39 | 4.92 |

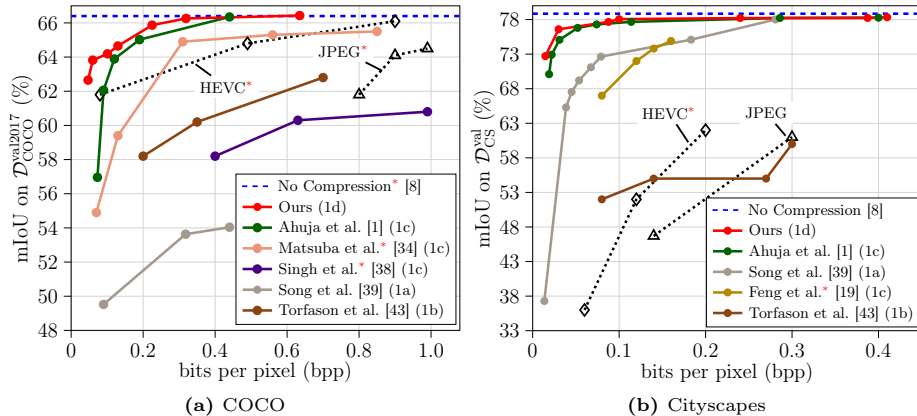


Fig. 5: Proposed JD approach ("Ours") against SOTA approaches on the mIoU metric for (a) $\mathcal{D}_{\text{COCO}}^{\text{val}2017}$ and (b) $\mathcal{D}_{\text{CS}}^{\text{val}}$ datasets. The values denoted by * are taken from respective papers and the identifiers in parentheses (1x) refer to the type of approach in Figure 1a ... 1d. On both COCO and Cityscapes datasets, our proposed approach "Ours" achieves better RD trade-off than SOTA baselines at a wide range of bitrates. Note that our proposed approach "Ours" uses $K = 1$ (COCO) and $K = 3$ (Cityscapes) in the ASPP block.

results are not necessarily exactly equal and may have a slight variation even for the same α in (3). Therefore, to obtain more reliable results, we averaged the RD values over three different seeds for exactly the same α .

Figure 5 shows the RD performance comparison of our proposed **JD** against recent SOTA and traditional codec baselines including JPEG [46] and HEVC [40]. Following the prior SOTA methods [1, 19, 34, 43], we choose **DeepLabv3** [8] with a **ResNet-50** [23] encoder as the **No Compression** baseline for both datasets. Further, on COCO, unlike JPEG, HEVC achieves better RD trade-off compared to learned image codec methods [39, 43] and compared to the feature compression approach by Singh et al. [38]. However, on Cityscapes, both perform worse than learning-based approaches. The existing SOTA baselines on feature compression by Matsuba et al. [34] and particularly Ahuja et al. [1] outperform conventional approaches (Figures 1a and 1b) on both datasets. In the figure, our proposed approach employs over-parameterization for both datasets, see Figure 4. Note

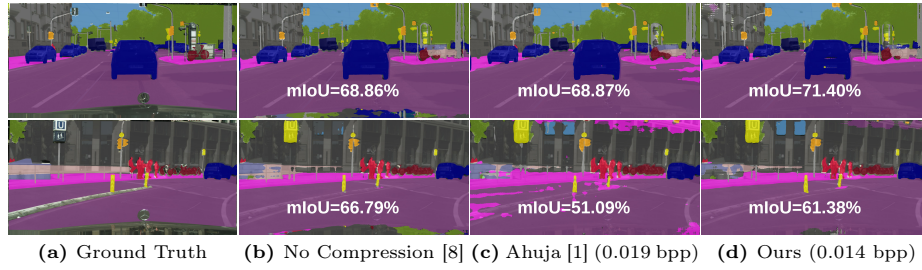


Fig. 6: Qualitative comparison of the proposed JD approach ("Ours") against Ahuja et al. [1] on two Cityscapes samples.

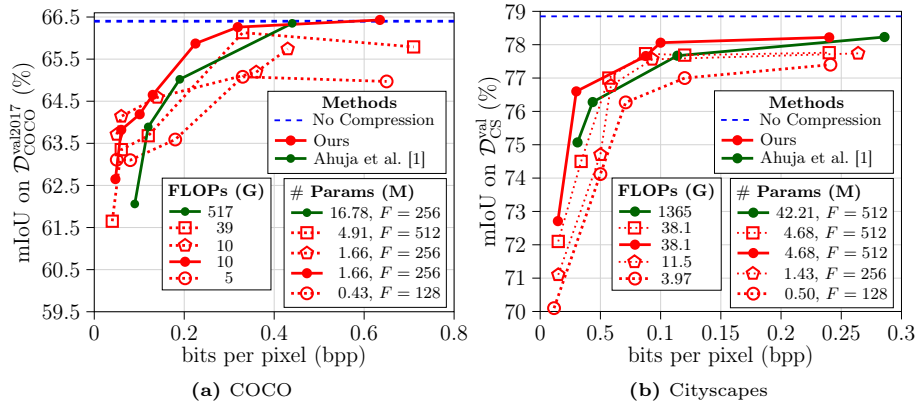


Fig. 7: Ablation study on the number F of feature maps of our proposed JD approach vs. the so-far SOTA approach Ahuja et al. [1]: Computational complexity per image and model size on (a) $\mathcal{D}_{\text{COCO}}^{\text{val}2017}$ and (b) $\mathcal{D}_{\text{CS}}^{\text{val}}$ datasets. Each marker type for our approach refers to a different number of feature maps F in the ASPP block of **JD**. All the curves—except "Ours"—are without over-parameterization in the ASPP block. This is why there is another $F = 256$ (COCO) and $F = 512$ (Cityscapes) configuration, respectively. Note that all methods with red curves use ($d = 5$, $d = 10$, $d = 15$) in the ASPP block, respectively.

that we also include results with a ResNet-101 encoder in the Supplement Figure 12 to better prove generalizability of our proposed **JD**.

Overall, our proposed **JD** outperforms all existing baselines, including the recent SOTA baseline Ahuja et al. [1], on the COCO dataset. Further, it also achieves the **No Compression** performance at a bitrate of 0.65 bpp. On Cityscapes, our method obtains superior performance in comparison to all baselines, while being comparable to Ahuja et al. [1] over a wide range of bitrates. As shown in Table 2, **JD** utilizes only 1.9% ... 2.8% of the FLOPs and 9.8% ... 11.59% of the number of parameters in comparison to the decoder functions **SD** and **D** by Ahuja et al. [1] on COCO and Cityscapes, respectively. As further information,

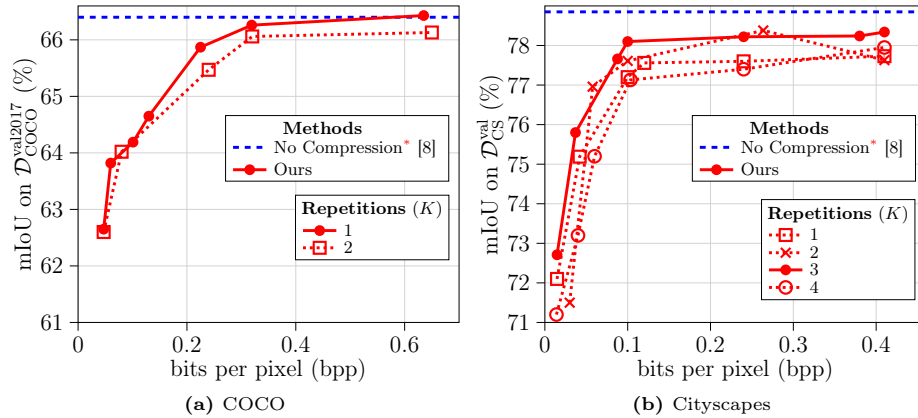


Fig. 8: Ablation study on the number of repetitions (K) for over-parameterization explained in Figure 4 in the proposed JD on (a) $\mathcal{D}_{\text{COCO}}^{\text{val}2017}$ and (b) $\mathcal{D}_{\text{CS}}^{\text{val}}$. Each marker type shows a different K in JD. Note that all methods use dilations ($d = 5, d = 10, d = 15$) and $F = 256$ (COCO) and $F = 512$ (Cityscapes) in the ASPP block, respectively.

edge device and total computational complexity (edge device plus cloud) are given in Supplement Tables 4 and 5.

Figure 6 presents a qualitative comparison of our proposed approach and the SOTA by Ahuja et al. [1] at very low bitrates, on two Cityscapes samples. As shown in Figures 6c and 6d, the proposed joint source and task decoding with training-time over-parameterization results in a significant reduction of misclassifications, especially in the predictions of object classes such as *sidewalks*, *road* and *poles*. More qualitative results are available in Supplement Section 5.

5.2 Ablation Studies

In the following, we perform ablation studies to investigate the robustness of the proposed JD. We start by varying the number of feature maps F in the ASPP block to investigate the effect of computational complexity on RD performance. Finally, we ablate over the training-time over-parameterization hyperparameter K to select the number of repetitions. Note that we also ablate over multiple dilation rates to select the dilation rate d in the ASPP dilated convolutional subblocks of JD as shown in Supplement Section 6.

Parameter selection: Figure 7 refers to the change in the number of output feature maps F in all convolutional layers of the JD ASPP block shown in Figure 3. It also results in the change of the size in the following pointwise convolution, which takes the concatenated output of the ASPP block. For a single setting, F remains the same for all convolutional layers in the ASPP block. By varying F , it is possible to achieve different JD computational complexities per image. We

ablate over $F \in \{128, 256, 512\}$ for both datasets. All curves, except "Ours", are without over-parameterization in the ASPP block.

As shown in Figure 7a, $F = 256$ is the best configuration for low bitrates. However, on higher bitrates, $F = 512$ performs better. To make a fair comparison with current baseline approaches [1, 34], we select $F = 256$ for further ablation studies on the COCO dataset. On Cityscapes, as shown in Figure 7b, we select $F = 512$ as it produces the best performance both at low and high bitrates. Note that the baselines on Cityscapes [1, 19] also utilize $F = 512$.

Number of repetitions in JD: Figure 8 depicts the ablation study to select the number of repetitions K for the over-parameterization (Figure 4) in the ASPP convolutional subblocks of **JD**. Each marker type shows a different number of repetitions in the subblocks of the ASPP block. We perform up to two repetitions on COCO and up to four repetitions on Cityscapes, respectively. As shown in Figure 8a, we observe that $K = 1$ produces a similar performance to $K = 2$ at low bitrates, but $K = 1$ is better at high bitrates on COCO. As shown in Figure 8b, $K = 3$ outperforms other curves in RD performance at most bitrates. Note that for COCO, our method at $K = 1$ already beats the previous SOTA [1], therefore we didn't perform a higher number of repetitions.

6 Conclusions

In this work, we show how *joint* source and task decoding can result in a highly efficient cloud DNN, while maintaining the same edge device computational complexity as the current SOTA for distributed semantic segmentation. This allows us to scale distributed semantic segmentation up to a large number of edge devices, without putting a high computational burden onto the cloud. Further, instead of applying training-time over-parameterization in the image encoder as suggested by [16, 44, 45], we demonstrate that by utilizing it in our proposed joint decoder **JD**, we further improve the performance in the high-bitrate regime. We achieve SOTA performance over a wide range of bitrates on the mean intersection over union metric, while using only 9.8% ... 11.59% of the cloud DNN parameters used in the previous SOTA on the semantically diverse COCO and Cityscapes datasets.

7 Limitations and Future Work

Since not all general semantic segmentation architectures are suitable for distributed deployment, current works only employ the DeepLabv3 network topology. Even though it is still considered as a very strong distributed semantic segmentation baseline [34], it is not a SOTA method in general semantic segmentation, as discussed in Section 2.1. As part of future work, we and the community should aim to bridge this gap by adapting existing general semantic segmentation approaches for such a distributed setting.

References



1. Ahuja, N., Datta, P., Kanzariya, B., Somayazulu, V.S., Tickoo, O.: Neural Rate Estimator and Unsupervised Learning for Efficient Distributed Image Analytics in Split-DNN Models. In: Proc. of the IEEE/CVF Conference on Computer Vision and Pattern Recognition (CVPR). pp. 2022–2030. Vancouver, BC, Canada (June 2023)
2. Anand, T., Sinha, S., Mandal, M., Chamola, V., Yu, F.R.: AgriSegNet: Deep Aerial Semantic Segmentation Framework for IoT-Assisted Precision Agriculture. *IEEE Sensors Journal* **21**(16), 17581–17590 (2021)
3. Ballé, J., Laparra, V., Simoncelli, E.P.: End-to-End Optimized Image Compression. In: Proc. of International Conference on Learning Representations (ICLR). Toulon, France (April 2017)
4. Ballé, J., Minnen, D., Singh, S., Hwang, S.J., Johnston, N.: Variational Image Compression With a Scale Hyperprior. arXiv preprint arXiv:1802.01436 (2018)
5. Bégin, J., Racapé, F., Feltman, S., Pushparaja, A.: CompressAI: A PyTorch Library and Evaluation Platform for End-to-End Compression Research. arXiv preprint arXiv:2011.03029 (2020)
6. Chakravarthy, A.S., Sinha, S., Narang, P., Mandal, M., Chamola, V., Yu, F.R.: DroneSegNet: Robust Aerial Semantic Segmentation for UAV-Based IoT Applications. *IEEE Transactions on Vehicular Technology* **71**(4), 4277–4286 (2022)
7. Chen, L.C., Papandreou, G., Kokkinos, I., Murphy, K., Yuille, A.L.: DeepLab: Semantic Image Segmentation With Deep Convolutional Nets, Atrous Convolution, and Fully Connected CRFS. *IEEE Transactions on Pattern Analysis and Machine Intelligence (TPAMI)* **40**(4), 834–848 (2017)
8. Chen, L.C., Papandreou, G., Schroff, F., Adam, H.: Rethinking Atrous Convolution for Semantic Image Segmentation. arXiv preprint arXiv:1706.05587 (2017)
9. Chen, L.C., Yang, Y., Wang, J., Xu, W., Yuille, A.L.: Attention to Scale: Scale-Aware Semantic Image Segmentation. In: Proc. of the IEEE Conference on Computer Vision and Pattern Recognition (CVPR). pp. 3640–3649. Las Vegas, NV, USA (June 2016)
10. Contributors, M.: MMSegmentation: OpenMMLab Semantic Segmentation Toolbox and Benchmark. <https://github.com/open-mmlab/mms Segmentation> (2020)
11. Cordts, M., Omran, M., Ramos, S., Rehfeld, T., Enzweiler, M., Benenson, R., Franke, U., Roth, S., Schiele, B.: The Cityscapes Dataset for Semantic Urban Scene Understanding. In: Proc. of the IEEE/CVF Conference on Computer Vision and Pattern Recognition (CVPR). pp. 3213–3223. Las Vegas, NV, USA (July 2016)
12. Dai, J., He, K., Sun, J.: Convolutional Feature Masking for Joint Object and Stuff Segmentation. In: Proc. of the IEEE Conference on Computer Vision and Pattern Recognition (CVPR). pp. 3992–4000. Boston, MA, USA (June 2015)
13. Dai, J., Qi, H., Xiong, Y., Li, Y., Zhang, G., Hu, H., Wei, Y.: Deformable Convolutional Networks. In: Proc. of the IEEE International Conference on Computer Vision (ICCV). pp. 764–773. Venice, Italy (October 2017)
14. Datta, P., Ahuja, N., Somayazulu, V.S., Tickoo, O.: A Low-Complexity Approach to Rate-Distortion Optimized Variable Bit-Rate Compression for Split DNN Computing. In: Proc. of 26th International Conference on Pattern Recognition (ICPR). pp. 182–188. IEEE, Montreal, QC, Canada (August 2022)
15. Ding, X., Zhang, X., Han, J., Ding, G.: Diverse Branch Block: Building a Convolution as an Inception-Like Unit. In: Proc. of the IEEE/CVF Conference on Computer Vision and Pattern Recognition (CVPR). pp. 10886–10895. virtual (June 2021)

16. Ding, X., Zhang, X., Ma, N., Han, J., Ding, G., Sun, J.: RepVGG: Making VGG-Style ConvNets Great Again. In: Proc. of the IEEE/CVF Conference on Computer Vision and Pattern Recognition (CVPR). pp. 13733–13742. virtual (June 2021)
17. Eshratifar, A.E., Abrishami, M.S., Pedram, M.: JointDNN: An Efficient Training and Inference Engine for Intelligent Mobile Cloud Computing Services. *IEEE Transactions on Mobile Computing* **20**(2), pp. 565–576 (2019)
18. Everingham, M., Van Gool, L., Williams, C.K.I., Winn, J., Zisserman, A.: The PASCAL Visual Object Classes Challenge 2012 (VOC2012) Results. <http://www.pascal-network.org/challenges/VOC/voc2012/workshop/index.html>
19. Feng, R., Jin, X., Guo, Z., Feng, R., Gao, Y., He, T., Zhang, Z., Sun, S., Chen, Z.: Image Coding for Machines With Omnipotent Feature Learning. In: Proc. of European Conference on Computer Vision (ECCV). pp. 510–528. Springer, Tel Aviv, Israel (October 2022)
20. Grauman, K., Darrell, T.: The Pyramid Match Kernel: Discriminative Classification With Sets of Image Features. In: Proc. of IEEE International Conference on Computer Vision (ICCV). vol. 2, pp. 1458–1465. Beijing, China (October 2005)
21. Guo, M.H., Lu, C., Hou, Q., Liu, Z., Cheng, M.M., Hu, S.: SegNeXt: Rethinking Convolutional Attention Design for Semantic Segmentation. *ArXiv abs/2209.08575* (2022), <https://api.semanticscholar.org/CorpusID:252367800>
22. Hariharan, B., Arbeláez, P., Girshick, R., Malik, J.: Hypercolumns for Object Segmentation and Fine-Grained Localization. In: Proc. of the IEEE Conference on Computer Vision and Pattern Recognition (CVPR). pp. 447–456. Boston, MA, USA (June 2015)
23. He, K., Zhang, X., Ren, S., Sun, J.: Deep Residual Learning for Image Recognition. In: Proc. of the IEEE/CVF Conference on Computer Vision and Pattern Recognition (CVPR). pp. 770–778. Las Vegas, NV, USA (July 2016)
24. Kang, B., Moon, S., Cho, Y., Yu, H., Kang, S.J.: MetaSeg: MetaFormer-Based Global Contexts-Aware Network for Efficient Semantic Segmentation. In: Proc. of the IEEE/CVF Winter Conference on Applications of Computer Vision (WACV). pp. 434–443. Waikoloa, HI, USA (January 2024)
25. Kingma, D.P., Welling, M.: Auto-Encoding Variational Bayes. *arXiv preprint arXiv:1312.6114* (2013)
26. Krizhevsky, A., Sutskever, I., Hinton, G.E.: ImageNet Classification With Deep Convolutional Neural Networks. *Communications of the ACM* **60**, pp. 84–90 (2012), <https://api.semanticscholar.org/CorpusID:195908774>
27. Langdon, G.G.: An Introduction to Arithmetic Coding. *IBM J. Res. Dev.* **28**(2), pp. 135–149 (march 1984). <https://doi.org/10.1147/rd.282.0135>, <https://doi.org/10.1147/rd.282.0135>
28. Lazebnik, S., Schmid, C., Ponce, J., et al.: Spatial Pyramid Matching. *Object Categorization: Computer and Human Vision Perspectives* **3**(4) (2009)
29. Lin, T., Maire, M., Belongie, S.J., Bourdev, L.D., Girshick, R.B., Hays, J., Perona, P., Ramanan, D., Doll’ar, P., Zitnick, C.L.: Microsoft COCO: Common Objects in Context. *CoRR abs/1405.0312* (2014), <http://arxiv.org/abs/1405.0312>
30. Liu, J., Sun, H., Katto, J.: Improving Multiple Machine Vision Tasks in the Compressed domain. In: Proc. of 26th International Conference on Pattern Recognition (ICPR). pp. 331–337. Montreal, QC, Canada (January 2022)
31. Liu, J., Sun, H., Katto, J.: Semantic Segmentation in Learned Compressed Domain. In: Proc. of Picture Coding Symposium (PCS). pp. 181–185. San Jose, CA, USA (December 2022)

32. Long, J., Shelhamer, E., Darrell, T.: Fully Convolutional Networks for Semantic Segmentation. In: Proc. of the IEEE Conference on Computer Vision and Pattern Recognition (CVPR). pp. 3431–3440. Boston, MA, USA (June 2015)
33. Matsubara, Y., Callegaro, D., Baidya, S., Levorato, M., Singh, S.: Head Network Distillation: Splitting Distilled Deep Neural Networks for Resource-Constrained Edge Computing Systems. *IEEE Access* **8**, 212177–212193 (2020)
34. Matsubara, Y., Yang, R., Levorato, M., Mandt, S.: Supervised Compression for Resource-Constrained Edge Computing Systems. In: Proc. of the IEEE/CVF Winter Conference on Applications of Computer Vision (WACV). pp. 2685–2695. Waikoloa, HI, USA (January 2022)
35. Minnen, D., Ballé, J., Toderici, G.: Joint Autoregressive and Hierarchical Priors for Learned Image Compression. In: Proc. of the 32nd International Conference on Neural Information Processing Systems (NeurIPS). p. 10794–10803 (December 2018)
36. Paszke, A., Gross, S., Massa, F., Lerer, A., Bradbury, J., Chanan, G., Killeen, T., Lin, Z., Gimelshein, N., Antiga, L., Desmaison, A., Köpf, A., Yang, E., DeVito, Z., Raison, M., Tejani, A., Chilamkurthy, S., Steiner, B., Fang, L., Bai, J., Chintala, S.: PyTorch: An Imperative Style, High-Performance Deep Learning Library. Red Hook, NY, USA (2019)
37. Sermanet, P., Eigen, D., Zhang, X., Mathieu, M., Fergus, R., LeCun, Y.: Overfeat: Integrated Recognition, Localization and Detection Using Convolutional Networks. arXiv preprint arXiv:1312.6229 (2013)
38. Singh, S., Abu-El-Haija, S., Johnston, N., Ballé, J., Shrivastava, A., Toderici, G.: End-to-End Learning of Compressible Features. In: Proc. of IEEE International Conference on Image Processing (ICIP). pp. 3349–3353. Abu Dhabi, United Arab Emirates (October 2020)
39. Song, M., Choi, J., Han, B.: Variable-Rate Deep Image Compression Through Spatially-Adaptive Feature Transform. In: Proc. of the IEEE/CVF International Conference on Computer Vision (ICCV). pp. 2380–2389. Montreal, QC, Canada (October 2021)
40. Sze, V., Budagavi, M., Sullivan, G.J.: High Efficiency Video Coding (HEVC): Algorithms and Architectures. Springer Publishing Company, Incorporated (2014)
41. Tang, X., Tu, W., Li, K., Cheng, J.: DFFNet: An IoT-Perceptive Dual Feature Fusion Network for General Real-Time Semantic Segmentation. *Information Sciences* **565**, 326–343 (2021)
42. Theis, L., Shi, W., Cunningham, A., Huszár, F.: Lossy Image Compression With Compressive Autoencoders. arXiv preprint arXiv:1703.00395 (2017)
43. Torfason, R., Mentzer, F., Agustsson, E., Tschannen, M., Timofte, R., Van Gool, L.: Towards Image Understanding from Deep Compression Without Decoding. arXiv preprint arXiv:1803.06131 (2018)
44. Vasu, P.K.A., Gabriel, J., Zhu, J., Tuzel, O., Ranjan, A.: MobileOne: An Improved One Millisecond Mobile Backbone. In: Proc. of the IEEE/CVF Conference on Computer Vision and Pattern Recognition (CVPR). pp. 7907–7917. Vancouver, BC, Canada (June)
45. Vasu, P.K.A., Gabriel, J., Zhu, J., Tuzel, O., Ranjan, A.: FastViT: A Fast Hybrid Vision Transformer using Structural Reparameterization. In: Proc. of the IEEE/CVF International Conference on Computer Vision (ICCV). pp. 5762–5772. Paris, France (October 2023)
46. Wallace, G.K.: The JPEG Still Picture Compression Standard. *Communications of the ACM* **34**(4), 30–44 (1991)

47. Wang, W., Dai, J., Chen, Z., Huang, Z., Li, Z., Zhu, X., Hu, X., Lu, T., Lu, L., Li, H., et al.: InternImage: Exploring Large-Scale Vision Foundation Models With Deformable Convolutions. In: Proc. of the IEEE/CVF Conference on Computer Vision and Pattern Recognition (CVPR). pp. 14408–14419. Orlando, FL, USA (June 2023)
48. Wang, W., Bao, H., Dong, L., Bjorck, J., Peng, Z., Liu, Q., Aggarwal, K., Mohammed, O.K., Singhal, S., Som, S., et al.: Image as a Foreign Language: BEiT Pretraining for All Vision and Vision-Language Tasks. arXiv preprint arXiv:2208.10442 (2022)
49. Wang, Z., Qin, M., Chen, Y.K.: Learning from the CNN-Based Compressed Domain. In: Proc. of the IEEE/CVF Winter Conference on Applications of Computer Vision (WACV). pp. 3582–3590. Virtual Event (January 2022)
50. Wu, Z., Shen, C., Hengel, A.v.d.: Bridging Category-Level and Instance-Level Semantic Image Segmentation. arXiv preprint arXiv:1605.06885 (2016)
51. Xie, E., Wang, W., Yu, Z., Anandkumar, A., Alvarez, J.M., Luo, P.: SegFormer: Simple and Efficient Design for Semantic Segmentation With Transformers. vol. 34, pp. 12077–12090. Virtual Event (December 2021)
52. Xue, T., Chen, B., Wu, J., Wei, D., Freeman, W.T.: Video Enhancement With Task-Oriented Flow. *International Journal of Computer Vision (IJCV)* **127**, 1106–1125 (2019)
53. Zhang, C., Bütepage, J., Kjellström, H., Mandt, S.: Advances in Variational Inference. *Proc. of IEEE Transactions on Pattern Analysis and Machine Intelligence (TPAMI)* **41**(8), 2008–2026 (2018)
54. Zhou, B., Zhao, H., Puig, X., Fidler, S., Barriuso, A., Torralla, A.: Scene Parsing Through ADE20k Dataset. In: Proc. of the IEEE Conference on Computer Vision and Pattern Recognition (CVPR). pp. 633–641. Honolulu, HI, USA (July 2017)

Supplementary: Distributed Semantic Segmentation with Efficient Joint Source and Task Decoding

Danish Nazir^{1,2}, Timo Bartels¹, Jan Piewek², Thorsten Bagdonat², and
Tim Fingscheidt¹

¹ Technische Universität Braunschweig, Braunschweig, Germany
{danish.nazir,timo.bartels,t.fingscheidt}@tu-bs.de

² Group Innovation, Volkswagen AG, Wolfsburg, Germany
{danish.nazir,jan.piewek,thorsten.bagdonat}@volkswagen.de

In the supplementary material, we provide a detailed overview of training and evaluation settings along with hyperparameters in Section 1. Further, in Section 2, we provide the topological details of the baseline approach and of our edge device processing (transmitter), followed by computational complexity discussion in Section 3. Section 4 provides additional rate-distortion (RD) results with a ResNet-101 encoder. Section 5 provides qualitative results on both COCO and Cityscapes datasets. Finally, Section 6 provides a dilation rate ablation study of our proposed joint decoder (**JD**) on both COCO and Cityscapes datasets.

1 Training Details

In the following section, we present a detailed description of the employed hyperparameters. Note that, for the ease of use and scalability, we integrated the **Compress-AI** library into the **MMSegmentation** toolbox to make a hybrid version and used it for conducting all of our experiments.

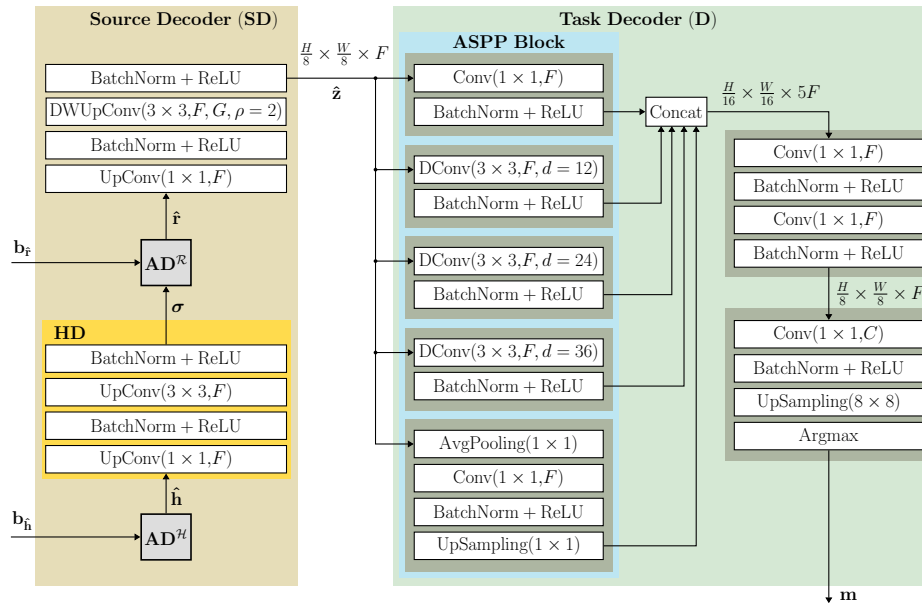
Optimization strategy: For all of our trainings, on both datasets, we utilize two optimizers, including the main optimizer and an auxiliary optimizer as suggested by **Compress-AI** [2, 3]. The **EntropyBottleneck.quantiles** parameter is optimized by the auxiliary optimizer, whereas remaining parameters are optimized by the main optimizer. We select **Adam** for both main and auxiliary optimizers. Further, except learning rate, all of the other parameters of both optimizers are exactly the same for both datasets.

Hyperparameters: We use Python v.3.8.10, PyTorch v.1.9.1, **MMSegmentation** v.1.0.0rc3 and **Compress-AI** v.0.8 for all our experiments. All of the hyperparameter details for reproducing our results are given in Table 3. Further, to conduct all our trainings, we utilized 4 NVIDIA-V100 GPUs and report the effective batch size. The polynomial learning rate schedule is given as follows:

$$\eta(\tau) = \eta_0 \left(1 - \frac{\tau}{\tau_{\max}} \right)^{0.9}, \quad (4)$$

Table 3: Settings and hyperparameters used for training on COCO and on Cityscapes.

| Setting/Hyperparameter | Cityscapes | COCO |
|--|------------------------|------------------------|
| # of training iterations | 80,000 | - |
| # of epochs | - | 42 |
| Initial LR (η_0) (main) | 0.001 | 0.01 |
| Initial LR (η_0) (aux) | 0.001 | 0.001 |
| Learning rate (LR) schedule $\eta_0(\tau)$ | polynomial (4) | polynomial (4) |
| Batch size | 8 | 16 |
| Random init | Kaiming initialization | Kaiming initialization |
| Clip grad type | norm | norm |
| Clip grad value | 1.0 | 1.0 |
| Optimizer parameters β_1, β_2 | 0.9, 0.99 | 0.9, 0.99 |
| Weight decay | 0 | 0 |

**Fig. 9: Receiver-sided architecture of Ahuja et al. [1]** with source decoder **SD** and task decoder **D** (see Figure 1c, and compare it to Figures 1d and 3)

with $\eta(\tau)$ being the learning rate at optimizer step τ and η_0 represents the initial learning rate given in Table 3. The maximum number of iterations/epochs are given by τ_{\max} .

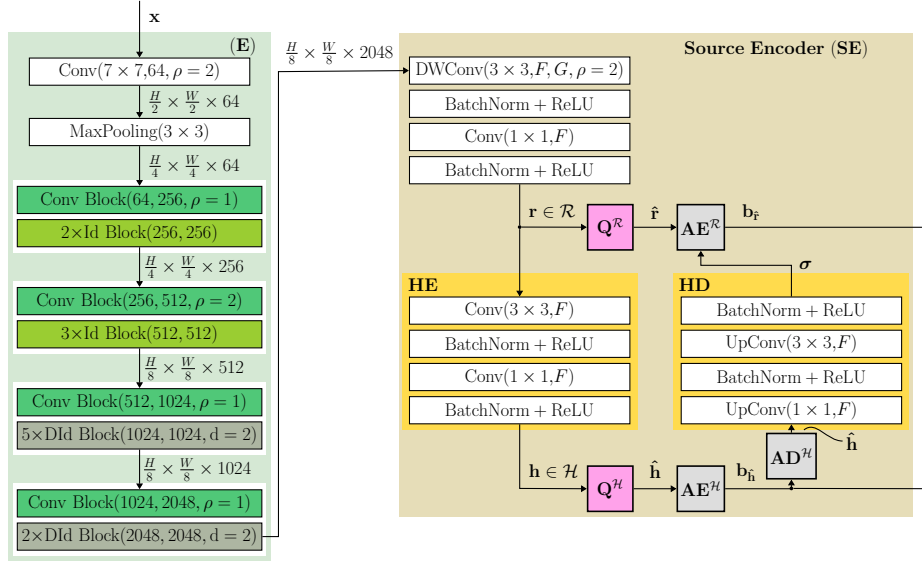


Fig. 10: Details of the **edge device processing (transmitter)** diagram with a semantic segmentation image encoder **E** and a source encoder **SE** in our experiments. This transmitter structure is used to generate the baseline results by Ahuja et al. [1] and by our proposal. The subblocks of **E** are drawn in Figure 11. For cloud processing (receiver), see Figure 9 for the baseline method by Ahuja et al. [1] and Figure 3 for our proposed approach.

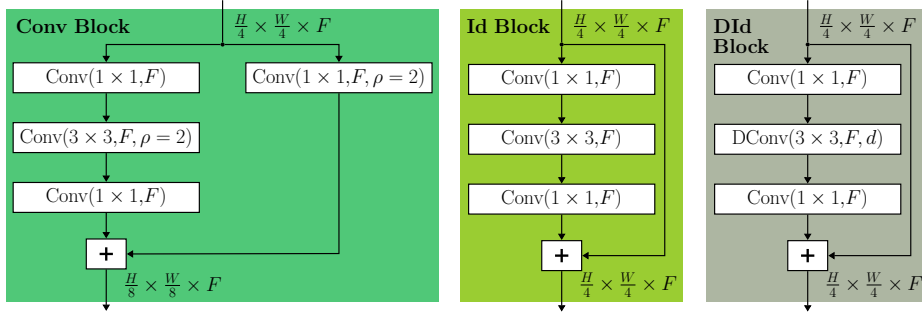


Fig. 11: Subblocks of the semantic segmentation image encoder **E**, see Figure 10.

2 Topology Details

In this section, we show the topological details of the receiver-sided architecture of the current state-of-the-art (SOTA) approach in Figure 9 and also our transmitter side in Figure 10.

Table 4: Comparison of FLOPs and number of parameters (edge DNNs)

| Methods | COCO | Cityscapes | #params (M) |
|--------------------------|-----------|------------|-------------|
| | FLOPs (G) | FLOPs (G) | |
| Song et al. [6] (1a) | 211 | 1687 | 18.77 |
| Torfason et al. [7] (1b) | 28 | 210 | 8.31 |
| Ahuja et al. [1] (1c) | 103 | 801 | 25.14 |
| Ours (1d) | 103 | 801 | 25.14 |

Table 5: Comparison of FLOPs and number of parameters (total computational complexity)

| Methods | COCO | | Cityscapes | |
|--------------------------|------------|--------------|------------|--------------|
| | FLOPs (G) | #params (M) | FLOPs (G) | #params (M) |
| Song et al. [6] (1a) | 1597 | 85.98 | 4521 | 112.07 |
| Torfason et al. [7] (1b) | 762 | 51.54 | 1363 | 77.63 |
| Ahuja et al. [1] (1c) | 624 | 41.92 | 2167 | 67.58 |
| Ours (1d) | 113 | 26.80 | 840 | 30.06 |

As shown in Figure 9, the receiver-sided architecture used by the current SOTA approach [1] comprises the entire source decoder (**SD**) and a separate task decoder (**D**). The **SD** contains in its upper part a grouped transposed convolutional block, with inputs $\hat{\mathbf{r}}$ and outputs $\hat{\mathbf{z}}$. After decoding, the compressed features $\hat{\mathbf{z}}$ are passed to the task decoder **D**, which outputs the semantic segmentation mask \mathbf{m} . Together, they form the cloud DNN of the method by Ahuja et al. [1]. Note that this structure deviates from our proposal (Figure 3) due to Ahuja’s sequential decoding of compressed features $\hat{\mathbf{z}}$ and semantic segmentation mask \mathbf{m} , leading to an increased computational complexity and suboptimal performance as compared to our proposal.

As illustrated in Figure 10, the edge device (transmitter) comprises a semantic segmentation image encoder **E** and a source encoder **SE**. The **SE** produces two bitstreams: the latent bitstream $\mathbf{b}_{\hat{\mathbf{r}}}$ and the hyperprior bitstream $\mathbf{b}_{\hat{\mathbf{h}}}$. These bitstreams are then transmitted to the cloud for processing. Additionally, the image encoder **E** follows the ResNet-50 [5] topology, with its subblocks depicted in Figure 11. The architecture of the identity (Id) block and the dilated identity (DId) blocks is identical, except that the DId block includes one dilated convolution layer.

3 Computational Complexity

In this section, we provide a comparison of the computational complexity incurred by the most relevant approaches on both, the edge device and in total (edge DNNs plus cloud DNNs).

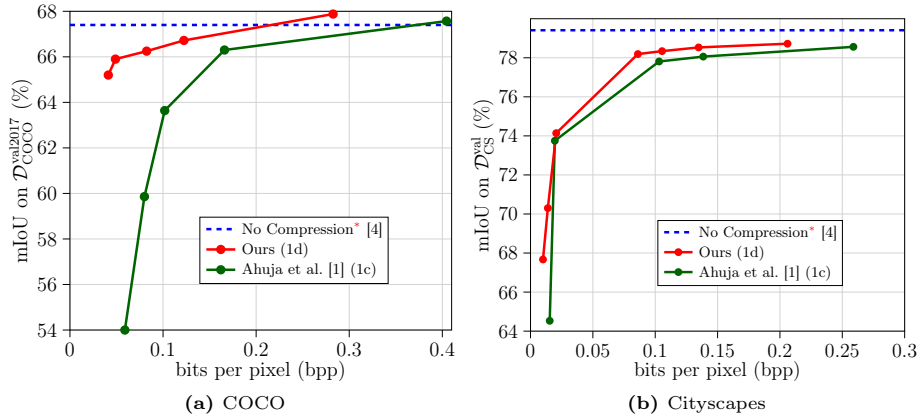


Fig. 12: Proposed JD approach ("Ours") against SOTA approach with a ResNet-101 encoder on the mIoU metric for (a) $\mathcal{D}_{\text{COCO}}^{\text{val}2017}$ and (b) $\mathcal{D}_{\text{CS}}^{\text{val}}$ datasets. The values denoted by * are taken from respective paper and the identifiers in parentheses (1x) refer to the type of approach in Figures 1c and 1d. On both COCO and Cityscapes datasets, our proposed approach "Ours" achieves better RD trade-off than SOTA baseline at a wide range of bitrates. Note that our proposed approach "Ours" uses $K = 1$ (COCO) and $K = 3$ (Cityscapes) in the ASPP block.

Table 4 presents the *edge device* computational complexity comparison of our approach against the baseline methods. Our proposed approach has the same edge device computational complexity as the so-far current state-of-the-art (SOTA) approach by Ahuja et al. [1]. Compared to Torfason et al. [7], both methods exhibit a clearly higher computational complexity and number of parameters. However, the decreased edge device computational complexity of Torfason et al. [7] results in inacceptably poor performance, as has been shown in Figures 5a and 5b. Note also that approaches following Figure 1b, such as Torfason et al. [7] transmit an image-coded bitstream which can be decoded at any point during transmission back to a reconstructed image, thereby being susceptible to data privacy fraud.

Table 5 illustrates a comparison of the *total* computational complexity of our approach against the baseline methods. Our proposed approach utilizes 18%/38% of the FLOPs and 63%/44% of the number of parameters in comparison to the SOTA by Ahuja et al. [1] on COCO/Cityscapes, respectively. Further, even though our approach exhibits higher edge computational complexity than the baseline by Torfason et al. [7], it significantly reduces the total computational complexity and utilizes only 14%/61% of the FLOPs and 51%/38% of the number of parameters on COCO/Cityscapes, respectively.



Fig. 13: Qualitative comparison of the proposed **JD** approach ("**Ours**") against Ahuja et al. [1] on the Cityscapes dataset at low bitrates.

4 Additional Results with a ResNet-101 Encoder

In this section, we present additional results with a ResNet-101 encoder on both COCO and Cityscapes to better prove the generalizability of our method. Figure 12 shows the rate-distortion (RD) performance of our proposed **JD** against the recent SOTA by Ahuja et al. [1]. Our proposed **JD** outperforms the SOTA approach on both COCO and Cityscapes. Further, it also exceeds the No Compression performance at a bitrate of 0.28 bpp on the COCO dataset.

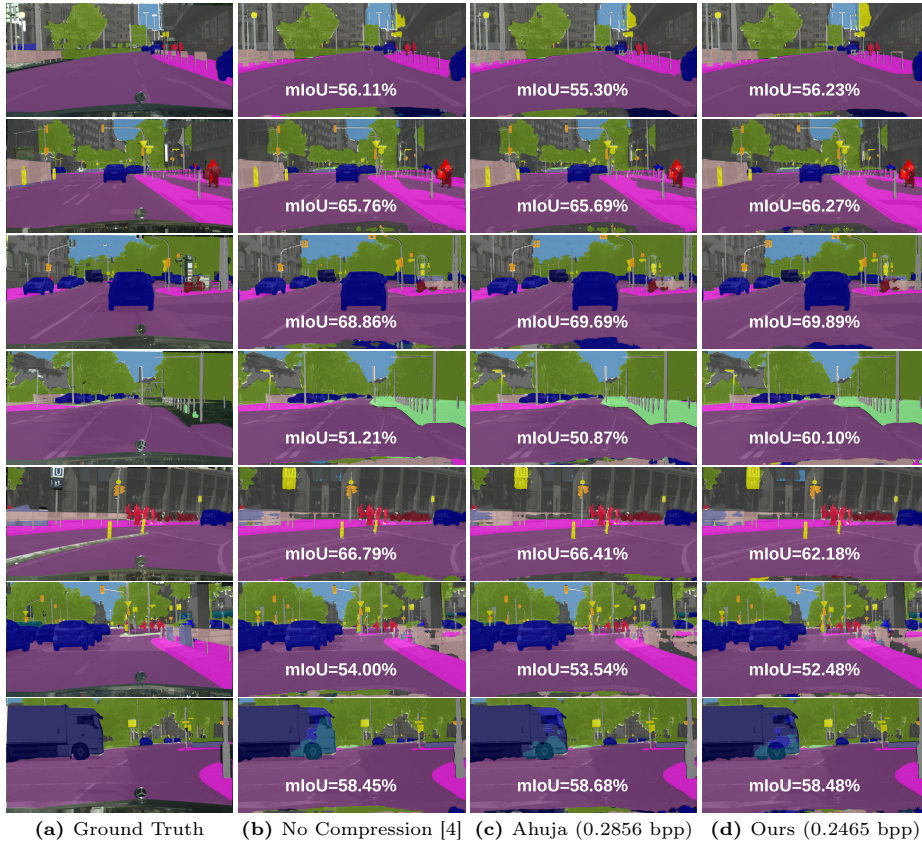


Fig. 14: Qualitative comparison of the **proposed JD approach ("Ours")** against **Ahuja et al. [1]** on the Cityscapes dataset **at high bitrates**.

Note that we use exactly the same settings (dilation rates and number of repetitions) in **JD** as in the case of the **ResNet-50** encoder.

5 Qualitative Results

In this section, we present a qualitative comparison with **ResNet-50** encoder against current SOTA [1] by Ahuja et al. [1] at low and high bitrates on both COCO and Cityscapes. In Figures 13 to 16, sample-individual *mIoU* performance is reported, while the *bitrates* of Ahuja et al. [1] and our proposal are given for the entire respective test set. Note that the bitrates of our method are always chosen to be lower.

Figure 13 shows for nine samples (organized in rows) a qualitative comparison of our proposed approach and Ahuja et al. [1] *at low bitrates on Cityscapes*. Rows 1 to 7 present strong cases for our method. Interestingly, in row 1, we also exceed

the **No Compression** baseline. Finally, rows 8 and 9 show the limitations of our method. In both cases, the mIoU is slightly worse, however, we do not observe missing classes such as *pedestrians*, *signs* and *cars*, which are considered critical for autonomous driving.

Similarly, Figure 14 also illustrates a qualitative comparison, but *at high bitrates on Cityscapes*. Rows 1 to 4 show strong examples for our method, whereas rows 5 to 7 depict limitations with slightly lower mIoU. Importantly, in rows 5 to 7, our approach does not remove important classes. Further, in rows 4 and 7, we also exceed the **No Compression** baseline.

Figure 15 depicts a qualitative comparison of our proposed approach and the method by Ahuja et al. [1] *at low bitrates on COCO*. We observe that all rows except the last represent the strong cases and our results are far superior than the method by Ahuja et al. [1]. Even in the last row, our results are comparable but our proposed approach fails to predict the background **persons** at a very small scale. Note that the approach of Ahuja et al. [1] also produces only partially correct predictions in the same region.

Figure 16 shows a qualitative comparison of our proposed approach and the method by Ahuja et al. [1] *at high bitrates on COCO*. At higher bitrates, we observe that our proposed approach provides comparable results to Ahuja et al. [1]. However, in rows 1 and 2, our proposed approach significantly reduces the false predictions of the classes including **cat** and **dog**. Further, it also does not omit the important classes such as **person** and **train**.

6 Dilation Rate Ablation

Figure 17 represents the dilation rate d ablation study in the ASPP dilated convolutional subblocks of **JD**. Each marker type shows a different dilation rate. Dilation enables the ASPP block to capture information at multiple scales, while achieving lower computational complexity [4]. We ablate over three dilation rates for both datasets. All curves, except "Ours", are without over-parameterization in the ASPP block. As shown in Figures 17a and 17b, we empirically found that the dilation rates ($d = 5$, $d = 10$, $d = 15$) in **JD** produce the best RD performance on both datasets.

References

1. Ahuja, N., Datta, P., Kanzariya, B., Somayazulu, V.S., Tickoo, O.: Neural Rate Estimator and Unsupervised Learning for Efficient Distributed Image Analytics in Split-DNN Models. In: Proc. of the IEEE/CVF Conference on Computer Vision and Pattern Recognition (CVPR). pp. 2022–2030. Vancouver, BC, Canada (June 2023)
2. Ballé, J., Minnen, D., Singh, S., Hwang, S.J., Johnston, N.: Variational Image Compression With a Scale Hyperprior. arXiv preprint arXiv:1802.01436 (2018)
3. Bégaint, J., Racapé, F., Feltman, S., Pushparaja, A.: CompressAI: A PyTorch Library and Evaluation Platform for End-to-End Compression Research. arXiv preprint arXiv:2011.03029 (2020)

4. Chen, L.C., Papandreou, G., Schroff, F., Adam, H.: Rethinking Atrous Convolution for Semantic Image Segmentation. arXiv preprint arXiv:1706.05587 (2017)
5. He, K., Zhang, X., Ren, S., Sun, J.: Deep Residual Learning for Image Recognition. In: Proc. of the IEEE/CVF Conference on Computer Vision and Pattern Recognition (CVPR). pp. 770–778. Las Vegas, NV, USA (July 2016)
6. Song, M., Choi, J., Han, B.: Variable-Rate Deep Image Compression Through Spatially-Adaptive Feature Transform. In: Proc. of the IEEE/CVF International Conference on Computer Vision (ICCV). pp. 2380–2389. Montreal, QC, Canada (October 2021)
7. Torfason, R., Mentzer, F., Agustsson, E., Tschannen, M., Timofte, R., Van Gool, L.: Towards Image Understanding from Deep Compression Without Decoding. arXiv preprint arXiv:1803.06131 (2018)

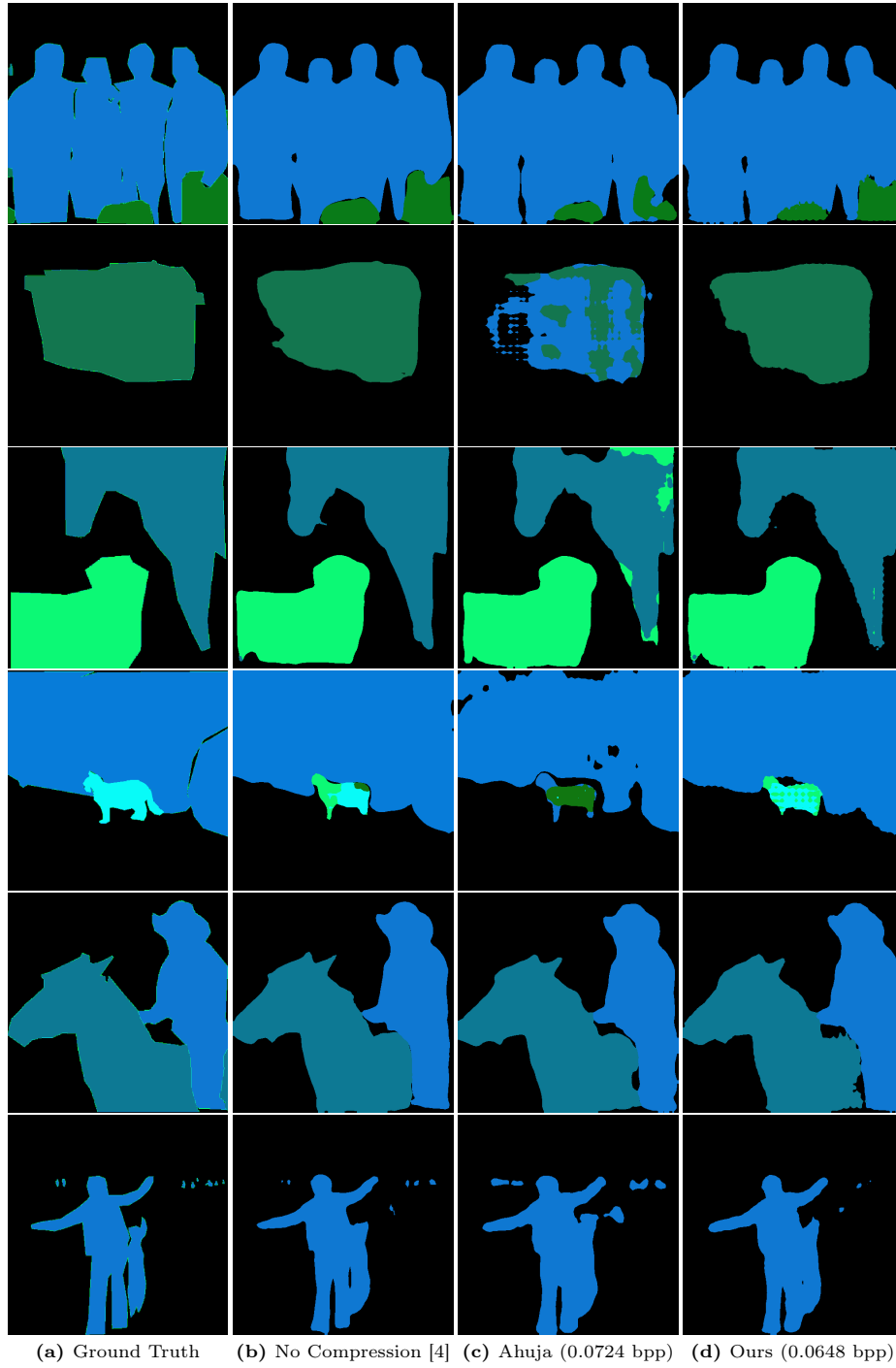


Fig. 15: Qualitative comparison of the **proposed JD approach ("Ours")** against Ahuja et al. [1] on the COCO dataset at low bitrates.

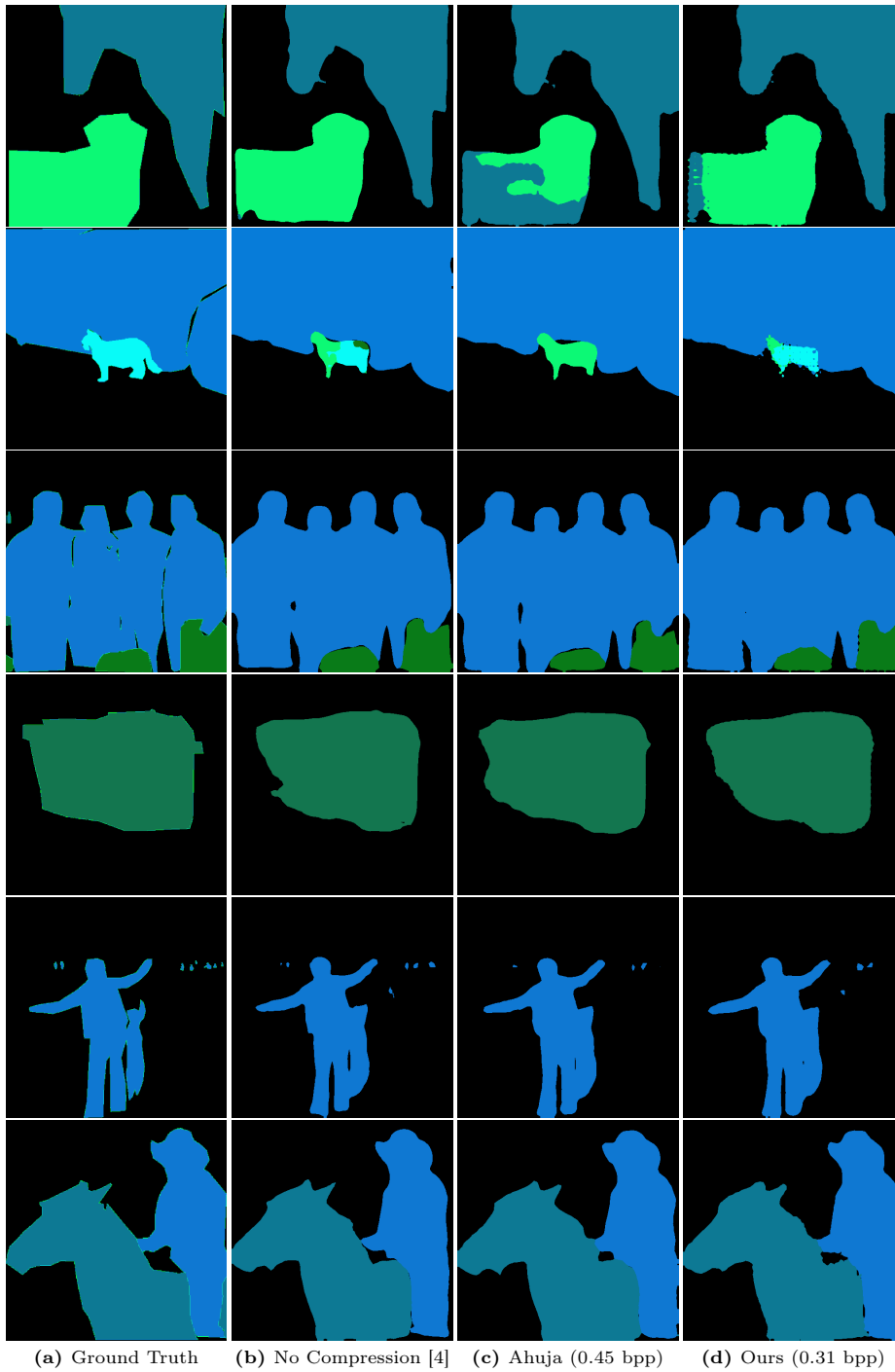


Fig. 16: Qualitative comparison of the **proposed JD approach ("Ours")** against Ahuja et al. [1] on the COCO dataset at high bitrates.

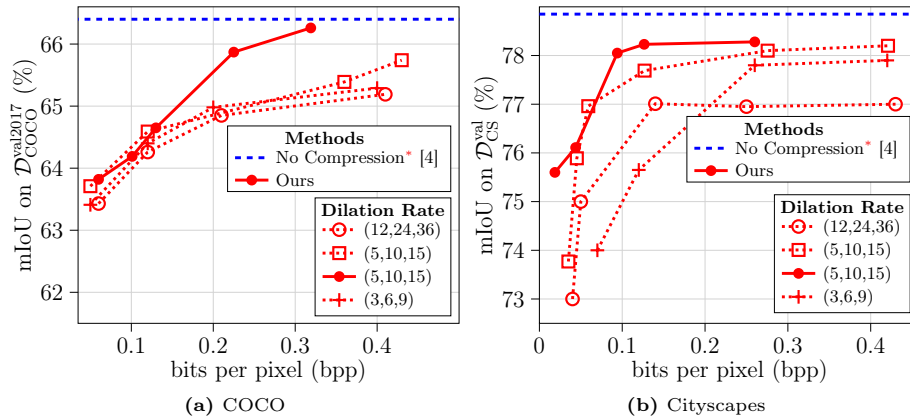


Fig. 17: Ablation study on ASPP dilation rates of our proposed JD approach on (a) $\mathcal{D}_{\text{COCO}}^{\text{val}2017}$ and (b) $\mathcal{D}_{\text{CS}}^{\text{val}}$. Each marker type shows a different dilation rate in the ASPP dilated convolutional subblocks of **JD**. Dilation rates, e.g., $(d = 5, d = 10, d = 15)$, refer to the spacing between the kernel elements in the respective dilated convolutional subblock of ASPP. All the curves—except "Ours"—are without overparameterization in the ASPP block. This is why there is another $(d = 5, d = 10, d = 15)$ configuration. Note that all methods use $F = 256$ (COCO) and $F = 512$ (Cityscapes) in the ASPP block, respectively